Expanded Molecular Imaging of Phytocompounds by Mass Spectrometry Using Novel On-Tissue Chemical Derivatization

Kevin J. Zemaitis,[a] Vivian Lin,[a] Amir H. Ahkami,[a] Tanya Winkler,[a] Christopher R. Anderton,[a] and Dušan Veličković1*[a]

[a] Earth and Biologicals Sciences Directorate
Pacific Northwest National Laboratory
Richland, WA, 99354, USA
*E-mail: dusan.velickovic@pnnl.gov

Keywords: mass spectrometry imaging (MSI) • on-tissue chemical derivatization (OTCD) • matrix-assisted laser desorption/ionization (MALDI) • phytohormones • phytocompounds

Abstract: Probing the entirety of any species metabolome is an analytical grand challenge, especially at a cellular scale. Where spatial metabolomics, completed primarily by matrix-assisted laser desorption/ionization (MALDI), has limited molecular coverage for several reasons. To expand the scope of spatial metabolomics, we developed an on-tissue chemical derivatization (OTCD) workflow using 4-APEBA for confident identification of several dozen elusive phytocompounds, including several phytohormones, which have various roles within stress responses and cellular communication. Superiority of 4-APEBA is established in comparison to other derivatization agents with (1) broad specificity towards carbonyls, (2) low background, and (3) introduction of bromine isotopes, where the latter two facilitate confident bioinformatics. The outlined workflow trailblazes a path towards spatial hormonomics within plant samples, enhancing detection of carboxylates, aldehydes, ketones, and plausibly phenols.

Introduction

There are an estimated 200,000 to 1 million distinct metabolites in the plant kingdom where any single plant species can produce tens of thousands of unique metabolites, far more than most other organisms.[1] However, only about 14,000 metabolites in the plant kingdom have been detected, suggesting that advanced analytical methods are needed to more thoroughly investigate such highly complex metabolomes.[2] This is even more evident at the level of single cells or single cell-types, where volumes and quantities of analytes are low and generally limit detection to only a small set of compounds.[3] Significant advancements in spatially-resolved and cell-specific metabolomics have emerged in the last decade,[3-4] and the use of these technologies have suggested a central role of cellular heterogeneity in biological systems (including plants) under different conditions where bulk measurements would mask relevant mechanistic insights. [3] One of the most utilized techniques for targeting and unveiling the cell-specific molecular signatures is matrix-assisted laser desorption/ionization (MALDI) mass spectrometry imaging (MSI).[4] MALDI-MSI has been applied for spatio-chemical analysis of polysaccharides,[5] glycans,[6] lipids,[7] proteins[8] and their proteoforms,[9] and various primary[10] and secondary metabolites[11] in plants.

Although widely applied in plant systems, a significant challenge remains in the ability of MALDI-MSI to measure and map many important phytocompounds. The lack of sensitivity towards these compounds is due, in part, to a number of factors that include their low mass, low abundance, low ionization yield, and tissue suppression effects, all of which limits the ability of current approaches to comprehensively describe the molecular makeup at the single cell level.[12] An additional challenge is that the broad physicochemical diversity of plant metabolites hinders their global analysis within any singular MSI workflow (e.g., using a single MALDI matrix, polarity, or mass range), and more comprehensive approaches have to be taken for broader

utility of MALDI-MSI. Recently, on-tissue chemical derivatization (OTCD) coupled with MALDI-MSI has emerged as a powerful approach to overcome sensitivity and other spectrometer limitations.[12-13] This approach enabled visualization of the spatial distribution of many biological compounds in microbial, plant, and mammalian cells, for the first time. Specifically, OTCD enhances the detection sensitivity by introducing a charged moiety or a readily ionizable functional group to the analyte. Concurrently, this derivatization process increases masses of the metabolites toward more sensitive regions, bypassing issues related to discrimination of metabolites from complex background spectral features (i.e., isobaric separation) and low mass transmission limitations of high-resolution mass spectrometers, such as Fourier transform ion cyclotron resonance mass spectrometry (FTICR-MS) instruments.

Various derivatization agents (DA) have been developed to target distinct functional groups of endogenous molecules.[12-13] For example, Girard's T (GT), Girard's P (GP), coniferyl alcohol (CA), and 2-picolyamine (PA) have been used for OTCD of carbonyl, amine, and carboxyl-containing compounds, respectively, in plant tissues, which enabled the detection of over six hundred unique metabolite features.[14] However, even though OTCD approaches with these DAs is promising, many challenges remain. For example, phytocompounds, including phytohormones, still remain undetected. Another issue is that the chemical composition of these DAs does not permit the ability to confidently distinguish between derivatized and non-derivatized MS signals.[14a, 15] Moreover, since many of these DAs are highly specific, it requires the use of multiple DAs to detect chemically diverse metabolites in a single run. Herein, we report an OTCD strategy using 4-(2-((4-bromophenethyl)dimethylammonium)ethoxy) benzenaminium dibromide (4-APEBA) that widely surpassed the benefits of conventional DAs used for carboxyl, aldehyde, and ketone derivatization. These three chemical moieties cover a very broad metabolic space, with a vast majority of plant metabolites containing at least one of these functional groups. 4-APEBA was initially introduced for electrospray ionization (ESI) workflows for derivatization of aldehydes.[16] A key advantage of this DA is the incorporation of a bromophenethyl group which introduces a distinctive isotopic signature of bromine to the derivative product ions, facilitating confident non-targeted detection and screening of derivatized compounds. In this work, we developed and optimized OTCD parameters for 4-APEBA deposition to enable simultaneous visualization and confident detection of unique phytohormones, amino acids, components of the TCA cycle, glycosides, etc., that were not observed by MALDI-MSI without derivatization or with previously reported DAs.

Results and Discussion

SCREENING DAS FOR A MODEL PHYTOHORMONE REVEALED THAT 4-APEBA SHOWED UNMATCHED POTENTIAL IN MALDI ANALYSES

Phytohormones are incredibly diverse within physiological function and functional groups present within their structures [17] We identified abscisic acid as a model target for phytohormone derivatization containing both a carboxyl and carbonyl functional group **(Fig. 1a)**. We began with several DAs **(Fig. 1b)** that could potentially enhance abscisic acid ionization efficiency and, more importantly, would be amenable to on-tissue deposition. Aside from 4-APEBA and previously reported DAs for MALDI[14b, 18], we also synthesized and tested 3-bromoactonyltrimethylammonium bromide (BTA). BTA had previously showed potential in derivatizing acidic plant hormones for capillary electrophoresis-MS analyses[19]. As OTCD is more challenging than in-solution analyses, these reagents were initially screened by ESI to identify stable DA product ions **(Figure 1c)**.

An ideal OTCD workflow should have a number of key attributes: (1) it should be performed under mild conditions, (2) provide a high reaction yield on-tissue, (3) prevent the delocalization of analytes, (4) preserve tissue integrity, and (5) provide

robust and reproducible results [12]. Through these experiments, we observed that 4-APEBA provided the greatest potential, with a significant sensitivity boost for derivatized abscisic acid, whereas BTA, GT, and DNPH provided enhancement, but were 1.6 to 2.9 log2-fold less responsive **(Fig. 1c)**. High derivatization yields for 4-APEBA, BTA, DNPH, and PA were also found, where non-derivatized abscisic acid was not detected for these DAs or were below the limit of detection. While GP and PA produced derivatized abscisic acid ions under these mild conditions, we observed the least significant boost in sensitivity at 4.2 and 4.3 log2-fold less than 4-APEBA, respectively. Conversely, N,N,N-trimethyl-2-(piperazin-1-yl)ethan-1-aminium iodide (TMPA) and N,N-dimethylpiperazine iodide (DMPI) were found to be ineffective in the tested conditions, and negligible differences in signal were seen compared to the control non-derivatized abscisic acid standard **(Fig. 1d)**. While the results for each of the eight in-solution DA trials will vary under different conditions, our data provided an essential first pass screening for mild conditions for evaluating the derivatization of phytohormones. For example, non-derivatized abscisic acid was detected within both GT and GP experiments, even though the molar ratios of these DAs were in vast excess for these reactions, signifying harsher conditions for derivatization are necessary. Additionally, several of the aforementioned DAs have previously be used for OTCD of carbonyl (DNPH[18a]) and carboxyl containing metabolites (TMPA[18b] and DMPI[18c]) under other conditions – but as stated above we opted to evaluate mild reaction conditions and avoided long exposures to high temperatures or organic solvents.

To evaluate the potential of the above DAs for MALDI-MSI, we profiled several of these reactions within dried droplet preparations. Due to high variability of dried droplet preparations for MALDI[20], we selected a subset of these DA reactions that performed well within the initial screening by ESI. This included both BTA and 4-APEBA and two commonly applied DAs in OTCD experiments, GP and GT. Several singular acquisitions were taken on dried droplets by MALDI, simulating singular pixels within imaging analysis for 4-APEBA, BTA, GP, and GT (**Fig. 2)**. Both 4-APEBA and BTA, which are novel OTCD DAs, showed the highest sensitivity enhancement for the derivatization product ions within MALDI experiments. Furthermore, 4-APEBA produced far fewer background peaks, with <325 peaks detected versus >3,000 peaks for all other DAs at a signal-to-noise threshold of 3. This is a notable advantage of 4-APEBA, as the vast complexity of spectral features poses a bioinformatics challenge for annotation of ion images based solely on high-resolution accurate mass detection.

Recently, the development of an open cloud annotation platform for MSI datasets, METASPACE, has helped facilitate non-targeted analysis of MSI data.[21] Within METASPACE, complex mass spectral features are annotated using a false discovery rate (FDR) framework that tremendously improves confidence, while expediting annotation of spatially resolved MS data.[14a] Additionally, by introducing a bromine atom into the analyte from the bromophenethyl of the 4-APEBA **(Fig. 2a)**, non-targeted OTCD approaches using METASPACE offer significantly higher confidence reinforced by the polyisotopic nature of bromine, where ^{79}Br and ^{81}Br have distinct relative abundance and an easily recognizable isotopic pattern.[15] Thus 4-APEBA, and other brominated DAs, reduce the likelihood of false derivatized annotations where underivatized endogenous compounds often are annotated as derivatized product ions without tandem MS confirmation.[14a] MALDI tandem MS was also evaluated for several standards **(Supporting Fig. S1)**, where common neutral losses were identified **(Supporting Table S1)** and generally, carboxyl standards were identified as molecular ions after loss of water and the 4-APEBA moiety and ketone and aldehyde compounds were identified as molecular ions after sole loss of the 4-APEBA moiety. For these reasons, we further focused on the development of 4-APEBA for OTCD for phytocompounds.

OPTIMIZED 4-APEBA DEPOSITION PERMITS SENSITIVE AND CONFIDENT ON-TISSUE CHEMICAL DERIVATIZATION AND CELL SPECIFIC IMAGING

There are various reasons that in-solution derivatization conditions are not directly applicable to MALDI-MSI preparation methods.[12] As mentioned above, OTCD application should be performed in a manner which preserves integrity of the tissue

and prevents delocalization of analytes, which are not considerations of in-solution approaches. Moreover, the tissue itself can cause various matrix effects and obfuscate detection of analytes. Given as such, the concentration of the DA and other reaction components (activator, catalyst, etc.) need to be balanced to obtain a high reaction yield, while avoiding signal delocalization, signal suppression, and tissue disruption. Additionally, solvent composition, reaction time, incubation, as well as the optimal pH for OTCD play a crucial role for successful imaging.[16b] Thus, we thoroughly evaluated protocols for OTCD using 4-APEBA and identified a two-step reaction which was optimal. This separates the activation of carboxylic acids, using EDC, and the derivatization of both analytes by 4-APEBA. Consequently, we also evaluated the quantity of reactants for the ideal EDC/4-APEBA ratio and evaluation of all conditions was completed primary based upon maximal sensitivity, delocalization, and molecular coverage from the analyzed plant tissues **(Fig. 3)**. To evaluate this, imaging analyses were carried out at a step size of 25 µm and 50 µm for poplar root and soybean root nodule sections, respectively.

Here we optimized our protocol using two plant systems to evaluate any biases that came from the biological tissues. The soybean root nodule (*Glycine max* inoculated with *Bradyrhizobium japonicum*) was selected because it represents a complex symbiotic system where bacterial-infected bacteroids, which fixate nitrogen, are heterogeneously dispersed among the uninfected plant cells. Roots from a non-nodulating plant species, poplar (*Populus spp*.), which host a variety of microorganisms capable of fixing nitrogen were also explored.[22] Poplar is also an important stock for bioenergy, as a wood product, and for environmental services,[23] as such mapping active metabolism and previously undiscovered phytocompounds within these root tissues is invaluable for future understanding of biotic and abiotic stresses. Several variable conditions for OTCD, outlined within **Supporting Table S2**, were evaluated against the METASPACE annotation quantity, the sensitivity of derivatized product detection, and detectable signal delocalization **(Fig. 3)**.

We used the KEGG database and a 10% FDR in METASPACE to determine the number of annotations for each condition. The relatively low FDR was selected because the introduction of 4-APEBA enabled high confidence annotations, due to unique isotopic patterns of derivatized compounds containing bromine **(Fig. 3d)**. Moreover, we found compounds annotated with FDRs >10% were mostly non-derivatized and/or false annotations. As a quality control measure for OTCD during optimization a standard of abscisic acid was spotted beside the tissue, and we used the relative intensity of derivatized abscisic acid signal to calculate the sensitivity of each analysis **(Fig. 3c)**. In such conditions, the intensity of the signal reflects the mutual effect of derivatization yield and suppression caused by the MALDI matrix and DA. Signal delocalization was quantified using our previously published procedure,[24] and we used it to determine the delocalization of both derivatized and non-derivatized molecules. Our data showed that optimal conditions, regardless of the plant tissue imaged, were obtained after depositing 16.66 µg/cm^2 of EDC followed by 5.56 µg/cm^2 of 4-APEBA within four spray cycles as outlined within the methods in **Supporting Information**. Subsequently, lower, or higher deposited amounts of EDC/4-APEBA, or combined spraying of EDC/4-APEBA, or a higher EDC/4-APEBA ratio caused unfavorable interactions on the sample and resulting in non-homogeneous matrix application, signal suppression, and signal delocalization to occur. This compatibility of applied DA with matrix and solvent system is essential for achieving homogeneous co-crystallization for detecting derivatized compounds and for producing high-fidelity cellular ion images.[12] This can be visualized in both spotted standards analysis **(Supporting Fig. S2)** and experiments on tissue **(Fig. 3a and 3b)**.

All tested conditions and ratios for OTCD are outlined within **Supporting Table S2**, and as mentioned above, optimized derivatization parameters were established at a calculated coverage of EDC to 4-APEBA of 3:1 (w:w) with maximal OTCD annotations resultant from deposition of 16.66 and 5.66 µg/cm^2 of EDC and 4-APEBA, respectively. This also resulted in the least amount of signal delocalization, which is crucial for the quality of MALDI images and their interpretation in a biological context. Interestingly, applying lower amounts of DAs increased delocalization **(Fig. 3a)**. While counterintuitive, because higher amounts of deposited DA require several more application cycles and more deposition of water onto the tissue, we postulate

that this observation could have resulted from low derivatization yield and ion suppression from other non-derivatized molecules. Further experiments were also performed with a solvent composition of 50% MeOH which did offer expanded coverage of several metabolites, including the phytohormone aminocyclopropane-carboxylate within poplar roots **(Supporting Fig. S3)**. Despite this, we observed differential amounts of sensitivity boost (i.e., derivatized lipoate, glyoxylate, and formate) in comparison to the optimized aqueous protocol, with a lower amount of phytocompounds annotated. These results were also found to be specific to tissue type, with drastically less annotations on soybean root nodules **(Supporting Table S2)**. This demonstrates the critical need to also evaluate the solvent system, as well as balance solvent composition for molecular coverage, sensitivity, delocalization, and DA stability for OTCD when approaching metabolomic workflows.

It should be noted that the entire optimization was also performed using DHB as a matrix, which itself contains a carboxyl group that can be derivatized. Indeed, we observed derivatized DHB as a major product ion within the imaging analyses alongside excess 4-APEBA, which can also serve as effective lock-mass calibrants. While this could impact ionization yields, with DHB being chemically altered, we also tested norharmane (NOR) as a matrix which has been great utility within dual polarity MALDI-MSI.[25] NOR contains no functional groups that could be derivatized by 4-APEBA, however, both sensitivity and molecular coverage for NOR deposition were significantly lower compared to DHB **(Supporting Fig. S4)**. This is further supported by ion images of non-derivatized components within OTCD experiments **(Supporting Fig. S6)**, suggesting that the derivatization of DHB did not negatively impact sensitivity, and can further act as a quality control measure for OTCD.

For further verification of successful OTCD by 4-APEBA, several standards of phytohormones and other plant metabolites containing aldehyde and carboxylate functional groups were subsequently activated, derivatized, and analyzed as dried droplets on a slide with the optimized parameters. As expected, all carboxyl-containing compounds showed intense derivatized signals with recognizable bromine isotopic patterns, and their underivatized forms were either not detected and/or below the limit of detection of the analyzed or were detected with less than 11.5 log2-fold lower signal. Notably, glucose showed a significantly enhanced derivatized signal with 5.2 log2-fold higher response than non-derivatized glucose, **(Supporting Table S3)**, indicating that 4-APEBA in our conditions also targets aldehydes. On the other hand, it seems that glycosides were poorly derivatized, as derivatized zeatin riboside was a very minor component of zeatin riboside spectrum **(Supporting Fig. S2a)**. We did also observe negligible double derivatization in molecules that contain multiple carboxyl groups (e.g., citric acid) within analyses but did not annotate any double derivatization for other molecules that have mixed chemical functionality (i.e., abscisic acid, jasmonic acid, and lignin model compounds) **(Supporting Table S3)**.

To further probe the duality of 4-APEBA OTCD, and key two-step activation with EDC, aromatic aldehydes and ketones produced in lignocellulose decay were also investigated with and without activation by EDC **(Supporting Fig. S2b)**. Without prior EDC deposition, the $[DHB+4\text{-}APEBA]^+$ product ion signal is significantly lower compared to two-step activation and derivatization. In contrast, all aldehyde and ketone standards tested showed intense derivatized product ions both with and without EDC deposition. Without EDC signal intensities were 0.7 to 9.3 log2-fold higher compared to signal in the presence of EDC **(Supporting Table S3)**, which is largely due to the suppression effects of the DA reaction byproducts and the vast excesses of both EDC and 4-APEBA. All non-derivatized signals of these compounds were observed at <10% relative intensity of the derivatized ions, demonstrating a significant boost in sensitivity after 4-APEBA derivatization. We also found an unexpected derivatization product with a standard of hydroquinone. Namely, several peaks with corresponding accurate mass matches to the brominated molecular formula of 4-APEBA attached to hydroquinone with a water loss **(Supporting Fig. S2c)**. As hydroquinone has two phenol groups and no carbonyls, it remains unclear the mechanism of derivatization by 4-APEBA, although oxidation of phenols is possible through several mechanisms.[26] Consequently, METASPACE annotations of phenol compounds should not be directly excluded as false, but rather further investigated. Overall, activation by EDC was found to be a necessary component for efficient derivatization of carboxylates with minor detrimental effects for other functional groups

targeted that do not need activation.[16a] These results signify a niche opportunity with DA specificity towards functional groups, which in the future can be exploited to image structural isomers by MALDI-MSI depending on the DA or sample preparation for OTCD.[27]

ON-TISSUE DEPOSITION OF 4-APEBA ENABLED HIGH-FIDELITY MAPPING OF PHYTOHORMONES AND PHYTOCHEMICALS

Finally, we applied our optimal 4-APEBA OTCD method to provide fine spatial information on more than 280 metabolites of different chemistries, polarities, and physiological roles from plant tissues. Detailed insight into the identity of these molecules can be seen in the **Supplementary Workbook**, where all endogenous MS features annotated as $[M+C_{18}H_{22}N_2Br]^+$ molecular ions from soybean root nodule and poplar root using KEGG and BraChem database at 10% FDR are shown. Besides the detection of important physiological aldehydes, ketones, and carboxylic acids, this approach provided broad detection of molecules with opposite acid/base chemistries in a single run. To date, to obtain similar coverage and visualize aldehydes, ketones, and carboxylic acids by MALDI-MSI, one either needed to use multiple DAs each specific for a unique functional group,[14b] or prepare multiple tissue sections with multiple matrices for separate imaging experiments. To exemplify the multiplexed capability of this OTCD approach, we revealed the spatial pattern of the critical respiratory substrate, pyruvate,[28] its decarboxylation product, acetaldehyde,[29] and stress reporter, glyoxylate **(Fig. 4).**[30] Due to their low molecular weights (88 Da, 44 Da, and 74 Da, respectively) these small metabolites have remained undetected in MSI experiments performed with FTICR-MS thus far. While other ambient ionization approaches have demonstrated the imaging of small metabolites,[31] comprehensive analyses of the pathways are always observed with far less coverage of the TCA cycle than shown via 4-APEBA OTCD **(Fig. 4)**. Moreover, the spatial resolution of these ambient imaging techniques is limited,[4] whereas MALDI-MSI has been applied with single cell resolution for nearly over a decade.

It is worth noting that using PA for OTCD, pyruvate was previously ascribed with a neutral loss [$-CO_2$] in the positive ion mode.[14b] Originally, this was annotated as an acetaldehyde-PA product ion, but as acetaldehyde is volatile, it was postulated that it was unlikely to be preserved in the plant tissue.[14b] Other early plant studies have also noted pyruvate in negative ion mode within root nodules.[32] However, these works and others to date used time-of-flight (TOF)-MS instrumentation for such measurements. While highly informative, imaging by MALDI-TOF can offer lower mass accuracy and mass resolution thus limiting the confidence of molecular annotations. Regardless, our results for the first time, shows a direct, clear, and confident image of pyruvate distribution in the tissue **(Fig. 4a)**. This workflow can be extremely valuable in tracking pyruvate kinetics in plants during respiration as an intermediary through glycolysis into gluconeogenesis. Other small aliphatic acids that are part of the TCA and glyoxalate cycles in plant were also observed, including cis-aconitate, α-ketoglutarate, fumarate, citrate/iso-citrate, malate, and succinate **(Fig. 4a).**[33]

We were also able to detect derivatized aliphatic acids with specific biological roles, such as allantonate, that serve as long-distance nitrogen transporters in soybean nodules **(Fig. 4b)**.[34] Numerous flavonol glycosides are also derivatized, with unique spatial distributions including malonyl-containing flavonol glycoside that was concentrated at the area of root attachment in the soybean root nodule **(Fig. 4b)**. Furthermore, we also detected malonate in soybean root nodules **(Fig. 4b)**. Malonate is an abundant C3-dicarboxylic acid in legumes, and its role in biological nitrogen fixation is highly contested: from a significant carbon source to a metabolic poison.[35] Importantly, this metabolite has not been observed within soybean root nodules via several different MSI capable methods previously used,[36] nor was it detected in other legume nodules.[32] Herein, revealing the high abundance of malonate in the outer layer of the infection zone might shed new light on its role in biological nitrogen fixation. The sensitivity of 4-APEBA OTCD also allowed visualization of other important phytocompounds, such as phytohormones and growth regulators,[37] which have been largely undetectable by all MSI methods. For example, we showed

the distribution of abscisic acid (**Supporting Fig. S5)**,[38] aminocyclopropane-carboxylate,[39] and salicylic acid[40] in poplar roots and abscisic acid, jasmonic acid, and methyl jasmonate[41] in soybean root nodules **(Fig. 4c)**.

This demonstrates the vast potential of 4-APEBA as a DA that enables detection of key phytocompounds, including phytohormones that are often present only in the trace amounts in individual cells. Routine non-targeted detection of these vital signaling molecules has not been feasible until now, even when state-of-the-art analytical techniques are employed.[37, 42] Under optimal conditions, where we addressed suppression effects from high concentrations of EDC/APEBA and poor matrix application, we can even measure non-derivatized molecules **(Supporting Fig. S6)** — albeit with less sensitivity than within non-derivatized control conditions. Thus, analyses are not limited solely to carboxyl, aldehyde, and ketone containing molecules from the derivatized tissue. This is exemplified by biogenic amines in soybean nodules that are synthesized by rhizobia to adapt to the plant cell environment **(Supporting Fig. S6)**.[43] Localization of these molecules remains the same after the OTCD protocol, which demonstrates that the preservation of native distributions of endogenous molecules.

Conclusions

OTCD methods are still in their infancy, but over the last half decade innovations in DAs and deposition methods have dramatically increased metabolic coverage that can be obtained at the cellular spatial scale. Our present study provides a leading-edge derivatization methodology that utilizes a novel OTCD agent, 4-APEBA, that enabled simultaneous boosts in sensitivity for amino acids, hormones, reducing sugars, aliphatic and aromatic carboxylic acids, aldehydes and ketones, and other primary and secondary metabolites with carbonyl groups. What particularly distinguishes this DA is the extremely low background and the incorporation of polyisotopic bromine into the derivative product ion. The latter permits an easily recognizable isotopic pattern during detection that facilitates confident non-targeted annotation. The optimized 4-APEBA workflow also demonstrates conditions are dependent on species or tissue type, and these analyses can occur at the cellular scale without signal delocalization. Furthermore, within a single imaging analysis, metabolites of opposite polarities and different hydrophobicity can be detected with negligible double derivatizations observed.

Although we demonstrated 4-APEBA applicability in plant root tissues, this approach is transferrable to microbial colonies or mammalians tissues as well. The two-step reaction within OTCD also revealed further potential for selective derivatization where aldehydes, ketones, and plausibly phenols are directly derivatized using 4-APEBA, whereas detection of carboxyl groups require prior activation for sensitive analyses. In summary, having demonstrated the *in-situ* profiling of key primary metabolites within several metabolic pathways, the application of 4-APEBA for the profiling of phytocompounds is a promising path forward for sensitive spatial metabolomics and hormonomics. Especially due to limited reported of several of these biologically important compounds and pathways which often required highly sensitive probes due to trace endogenous levels.

Acknowledgements

This research was performed on a project award doi.org/10.46936/intm.proj.2021.60091/60001441 (D.V.) from the Environmental Molecular Sciences Laboratory, a Department of Energy (DOE) Office of Science User Facility sponsored by the Biological and Environmental Research program under Contract No. DE-AC05-76RL01830.

Author Contributions:

D.V. conceptualized the study and supervised the project. K.J.Z. performed derivatization and MALDI-MSI experiments. K.J.Z. and D.V. performed data analysis and visualization. V.L. synthesized derivatization agents. A.A. and T.W. generated and provided poplar plants for experiments. D.V. acquired funding for the project. K.J.Z. and D.V. wrote the initial manuscript with V.L., A.A., T.W., and C.R.A. providing input. All authors edited the manuscript.

Data availability:

All annotations and ion images can be found in the METASPACE project:

https://metaspace2020.eu/api_auth/review?prj=f8500888-401a-11ed-89bf-4f62674f048b&token=JvizK2A5QuJo

References

[1] C. Y. Fang, A. R. Fernie, J. Luo, *Trends Plant Sci* **2019**, *24*, 83-98.

[2] R. Katam, C. W. Lin, K. Grant, C. S. Katam, S. X. Chen, *Int J Mol Sci* **2022**, *23*.

[3] L. P. de Souza, M. Borghi, A. Fernie, *Int J Mol Sci* **2020**, *21*.

[4] M. J. Taylor, J. K. Lukowski, C. R. Anderton, *J Am Soc Mass Spectr* **2021**, *32*, 872-894.

[5] D. Velickovic, D. Ropartz, F. Guillon, L. Saulnier, H. Rogniaux, *J Exp Bot* **2014**, *65*, 2079-2091.

[6] D. Velickovic, Y. C. Liao, S. Thibert, M. Velickovic, C. Anderton, J. Voglmeir, G. Stacey, M. W. Zhou, *Front Plant Sci* **2022**, *13*.

[7] D. Sturtevant, M. Aziz, T. B. Romsdahl, C. D. Corley, K. D. Chapman, *Methods Mol Biol* **2021**, *2295*, 417-438.

[8] H. Q. Liu, M. M. Han, J. M. Li, L. Qin, L. L. Chen, Q. C. Hao, D. X. Jiang, D. F. Chen, Y. Y. Ji, H. Han, C. L. Long, Y. J. Zhou, J. C. Feng, X. D. Wang, *Anal Chem* **2021**, *93*, 11920-11928.

[9] M. Zhou, J. M. Fulcher, K. J. Zemaitis, D. D. J, L. Y-C, M. Velickovic, D. Velickovic, L. Bramer, W. R. Kew, G. Stacey, L. Pasa-Tolic, *Front. Anal. Sci.* **2022**, *2*, 1012707.

[10] Y. H. Dong, P. Sonawane, H. Cohen, G. Polturak, L. Feldberg, S. H. Avivi, I. Rogachev, A. Aharoni, *New Phytol* **2020**, *228*, 1986-2002.

[11] D. Velickovic, H. L. Liao, R. Vilgalys, R. K. Chu, C. R. Anderton, *J Nat Prod* **2019**, *82*, 1382-1386.

[12] M. Merdas, M. Lagarrigue, Q. Vanbellingen, T. Umbdenstock, G. Da Violante, C. Pineau, *J Mass Spectrom* **2021**, *56*.

[13] aC. Harkin, K. W. Smith, F. L. Cruickshank, C. L. Mackay, B. Flinders, R. M. A. Heeren, T. Moore, S. Brockbank, D. F. Cobice, *Mass Spectrom Rev* **2021**; bQ. Q. Zhou, A. Fulop, C. Hopf, *Anal Bioanal Chem* **2021**, *413*, 2599-2617; cH. Yang, C. E. Chandler, S. N. Jackson, A. S. Woods, D. R. Goodlett, R. K. Ernst, A. J. Scott, *Anal Chem* **2020**, *92*, 13667-13671.

[14] aE. A. Larson, T. T. Forsman, L. Stuart, T. Alexandrov, Y. J. Lee, *Anal Chem* **2022**, *94*, 8983-8991; bM. E. Duenas, E. A. Larson, Y. J. Lee, *Front Plant Sci* **2019**, *10*.

[15] R. Shariatgorji, A. Nilsson, N. Strittmatter, T. Vallianatou, X. Q. Zhang, P. Svenningsson, R. J. A. Goodwin, P. E. Andren, *J Am Soc Mass Spectr* **2020**, *31*, 2553-2557.

[16] aM. Eggink, M. Wijtmans, A. Kretschmer, J. Kool, H. Lingeman, I. J. P. de Esch, W. M. A. Niessen, H. Irth, *Anal Bioanal Chem* **2010**, *397*, 665-675; bA. Kretschmer, M. Giera, M. Wijtmans, L. de Vries, H. Lingeman, H. Irth, W. M. A. Niessen, *J Chromatogr B* **2011**, *879*, 1393-1401.

[17] aS. Ogawa, S. K. Cui, A. R. F. White, D. C. Nelson, S. Yoshida, K. Shirasu, *Nat Commun* **2022**, *13*; bH. W. Jing, D. A. Korasick, R. J. Emenecker, N. Morffy, E. G. Wilkinson, S. K. Powers, L. C. Strader, *Nat Commun* **2022**, *13*; cT. T. Zhu, C. Herrfurth, M. M. Xin, T. Savchenko, I. Feussner, A. Goossens, I. De Smet, *Nat Commun* **2021**, *12*; dA. Kokla, M. Leso, X. Zhang, J. Simura, P. T. Serivichyaswat, S. K. Cui, K. Ljung, S. Yoshida, C. W. Melnyk, *Nat Commun* **2022**, *13*.

[18] aB. Flinders, J. Morrell, P. S. Marshall, L. E. Ranshaw, M. R. Clench, *Anal Bioanal Chem* **2015**, *407*, 2085-2094; bC. Sun, W. Liu, Y. Geng, X. Wang, *Anal Chem* **2020**, *92*, 12126-12131; cS. S. Wang, Y. J. Wang, J. Zhang, T. Q. Sun, Y. L. Guo, *Anal Chem* **2019**, *91*, 4070-4076.
[19] M. L. Chen, Y. Q. Huang, J. Q. Liu, B. F. Yuan, Y. Q. Feng, *J Chromatogr B* **2011**, *879*, 938-944.
[20] Y. K. Choi, J. Y. Oh, S. Y. Han, *J Am Soc Mass Spectr* **2018**, *29*, 2003-2011.
[21] A. Palmer, P. Phapale, I. Chernyavsky, R. Lavigne, D. Fay, A. Tarasov, V. Kovalev, J. Fuchser, S. Nikolenko, C. Pineau, M. Becker, T. Alexandrov, *Nat Methods* **2017**, *14*, 57-60.
[22] S. L. Doty, A. W. Sher, N. D. Fleck, M. Khorasani, R. E. Bumgarner, Z. Khan, A. W. K. Ko, S. H. Kim, T. H. DeLuca, *Plos One* **2016**, *11*.
[23] aX. H. Yang, U. C. Kalluri, S. P. DiFazio, S. D. Wullschleger, T. J. Tschaplinski, Z. M. Cheng, G. A. Tuskan, *Crit Rev Plant Sci* **2009**, *28*, 285-308; bT. Varga, K. K. Hixson, A. H. Ahkami, A. W. Sher, M. E. Barnes, R. K. Chu, A. K. Battu, C. D. Nicora, T. E. Winkler, L. R. Reno, S. C. Fakra, O. Antipova, D. Y. Parkinson, J. R. Hall, S. L. Doty, *Front Plant Sci* **2020**, *11*.
[24] D. Velickovic, K. Sharma, T. Alexandrov, J. B. Hodgin, C. R. Anderton, *J Am Soc Mass Spectr* **2022**, *33*, 1577-1580.
[25] aA. Treu, A. Rompp, *Rapid Commun Mass Sp* **2021**, *35*; bM. Vandenbosch, S. P. Nauta, A. Svirkova, M. Poeze, R. M. A. Heeren, T. P. Siegel, E. Cuypers, M. Marchetti-Deschmann, *Anal Bioanal Chem* **2021**, *413*, 2683-2694.
[26] R. Pinnataip, B. P. Lee, *Acs Omega* **2021**, *6*, 5113-5118.
[27] D. Velickovic, M. W. Zhou, J. S. Schilling, J. W. Zhang, *J Fungi* **2021**, *7*.
[28] A. H. Millar, J. Whelan, K. L. Soole, D. A. Day, *Annu Rev Plant Biol* **2011**, *62*, 79-104.
[29] I. Ventura, L. Brunello, S. Iacopino, M. C. Valeri, G. Novi, T. Dornbusch, P. Perata, E. Loreti, *Sci Rep-Uk* **2020**, *10*.
[30] A. Zarei, C. J. Brikis, V. S. Bajwa, G. Z. Chiu, J. P. Simpson, J. R. DeEll, G. G. Bozzo, B. J. Shelp, *Front Plant Sci* **2017**, *8*.
[31] L. E. Flint, G. Hamm, J. D. Ready, S. Ling, C. J. Duckett, N. A. Cross, L. M. Cole, D. P. Smith, R. J. A. Goodwin, M. R. Clench, *Anal Chem* **2020**, *92*, 12538-12547.
[32] H. Ye, E. Gemperline, M. Venkateshwaran, R. B. Chen, P. M. Delaux, M. Howes-Podoll, J. M. Ane, L. J. Li, *Plant J* **2013**, *75*, 130-145.
[33] Y. J. Zhang, A. R. Fernie, *J Integr Plant Biol* **2018**, *60*, 1199-1216.
[34] S. W. Thu, M. Z. Lu, A. M. Carter, R. Collier, A. Gandin, C. C. Sitton, M. Tegeder, *J Exp Bot* **2020**, *71*, 4495-4511.
[35] R. Karunakaran, A. K. East, P. S. Poole, *Appl Environ Microb* **2013**, *79*, 4496-4498.
[36] aB. J. Agtuca, S. A. Stopka, S. Evans, L. Samarah, Y. Liu, D. Xu, M. G. Stacey, D. W. Koppenaal, L. Pasa-Tolic, C. R. Anderton, A. Vertes, G. Stacey, *Plant J* **2020**, *103*, 1937-1958; bL. Z. Samarah, R. Khattar, T. H. Tran, S. A. Stopka, C. A. Brantner, P. Parlanti, D. Velickovic, J. B. Shaw, B. J. Agtuca, G. Stacey, L. Pasa-Tolic, N. Tolic, C. R. Anderton, A. Vertes, *Anal Chem* **2020**, *92*, 7289-7298; cD. Velickovic, B. J. Agtuca, S. A. Stopka, A. Vertes, D. W. Koppenaal, L. Paga-Tolic, G. Stacey, C. R. Anderton, *Isme J* **2018**, *12*, 2335-2338.
[37] Y. H. Wang, H. R. Irving, *Plant Signal Behav* **2011**, *6*, 494-500.
[38] D. Yu, H. Wildhagen, S. Tylewicz, P. C. Miskolczi, R. P. Bhalerao, A. Polle, *New Phytologist* **2019**, *223*, 1192-1203.
[39] J. K. Polko, J. J. Kieber, *Front Plant Sci* **2019**, *10*.
[40] C. Ullah, C.-J. Tsai, S. B. Unsicker, L. Xue, M. Reichelt, J. Gershenzon, A. Hammerbacher, *New Phytologist* **2019**, *221*, 960-975.
[41] A. Zdyb, K. Demchenko, J. Heumann, C. Mrosk, P. Grzeganek, C. Göbel, I. Feussner, K. Pawlowski, B. Hause, *New Phytologist* **2011**, *189*, 568-579.

[42] L. Y. Wang, Y. L. Zou, H. Y. Kaw, G. Wang, H. Z. Sun, L. Cai, C. Y. Li, L. Y. Meng, D. H. Li, *Plant Methods* **2020**, *16*.
[43] S. Fujihara, *Microbes Environ* **2009**, *24*, 1-13.

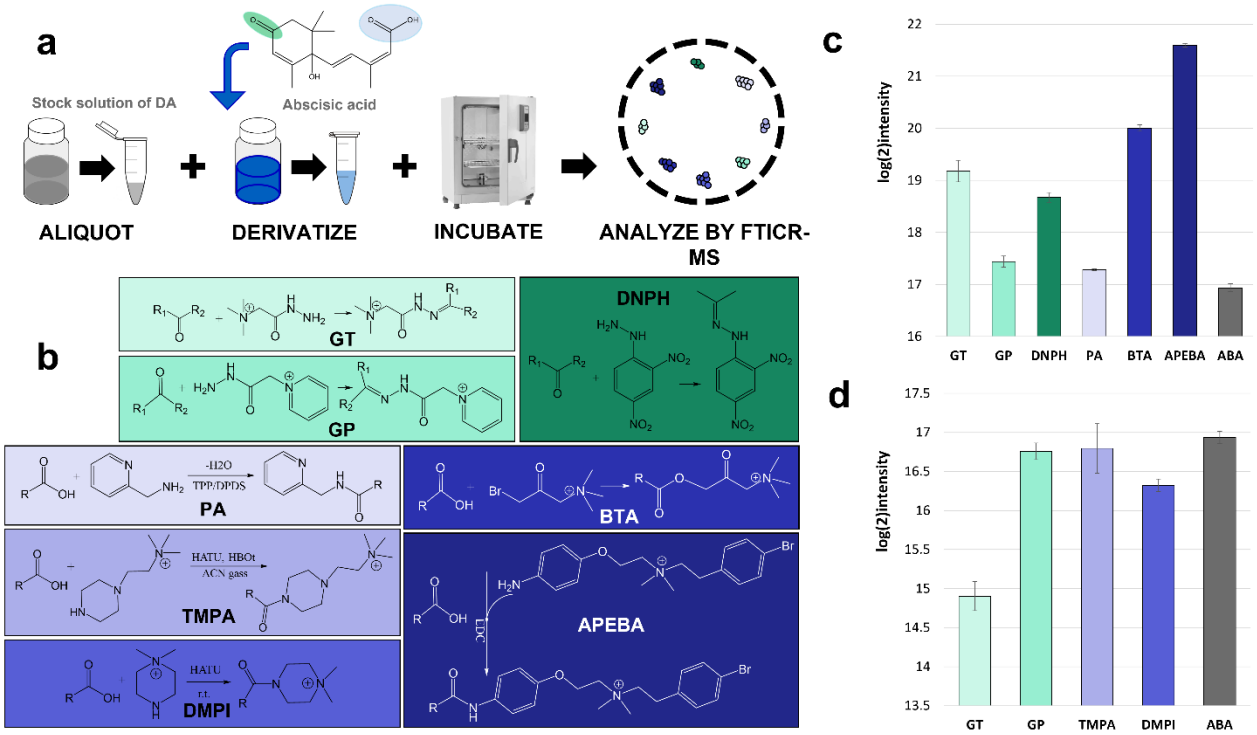

Fig. 1 Testing efficacy of various DAs by ESI-FTICR-MS. **a** Workflow used for screening derivatization reactions using abscisic acid as a model phytohormone. **b** Reaction scheme for all the DAs tested within this study and their respective color coding. **c** Sensitivity boost due to derivatization noted within ESI FTICR-MS measurements, where the signal intensity is log2 scaled for the different product ions of abscisic acid and compared against the abscisic acid standard. **d** Relative intensity of non-derivatized abscisic acid detected across all reactions tested where if not listed abscisic acid was either fully reacted or below the limit of detection of the analyzer.

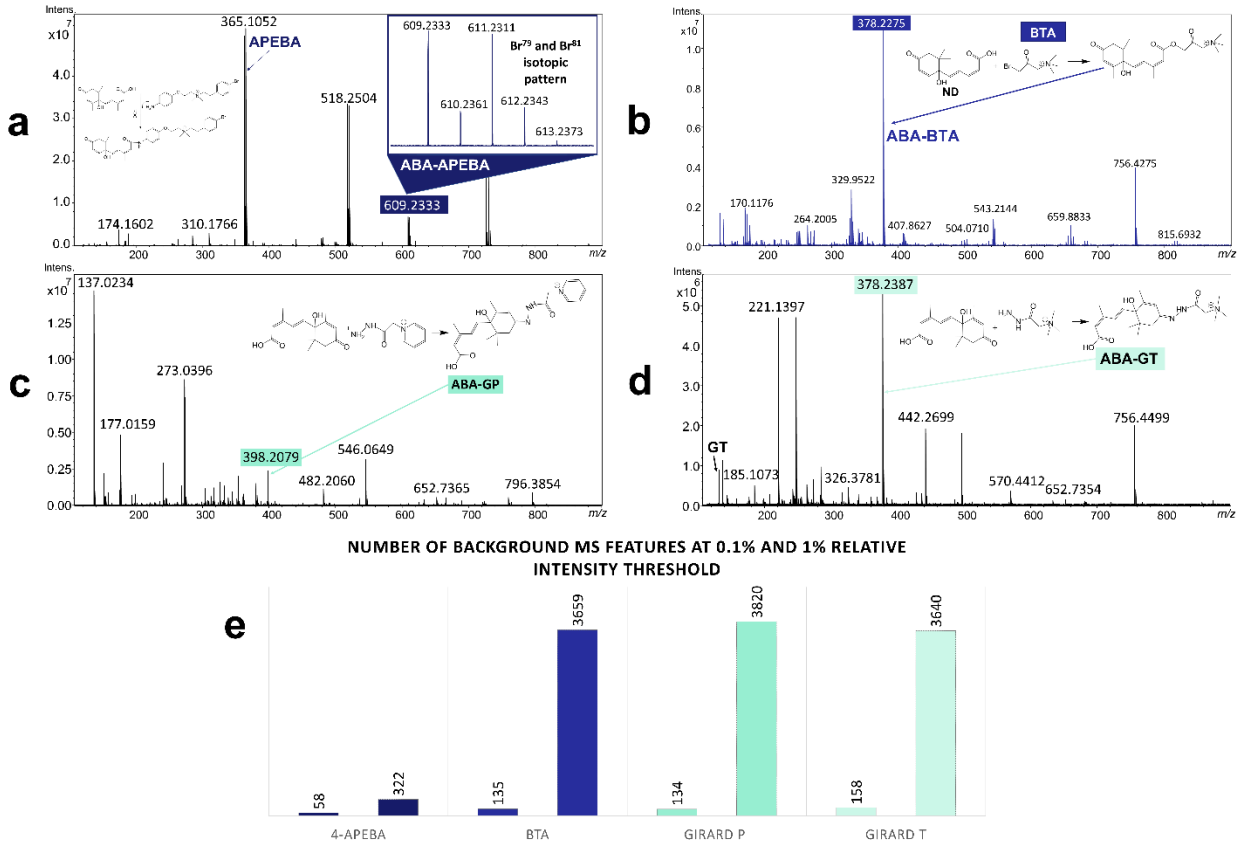

Fig. 2 MALDI mass spectra of different derivatization reactions of abscisic acid using DHB as a MALDI matrix. Experiments were completed to identify the expected background within a singular pixel in an imaging analysis. **a** MALDI mass spectrum of derivatization reaction products using 4-APEBA. Note that within the zoomed inset, a bromine isotopic pattern can be discerned in the 4-APEBA abscisic acid product ion. **b** MALDI mass spectrum of derivatization reaction products using BTA. **c** MALDI mass spectrum of derivatization reaction products using GP. **d** MALDI mass spectrum of derivatization reaction products using GT. **e** Number of MS peaks with a signal-to-noise threshold of 3 at 1% and 0.1% relative intensity thresholds, where more complex signal background complicates downstream analyses.

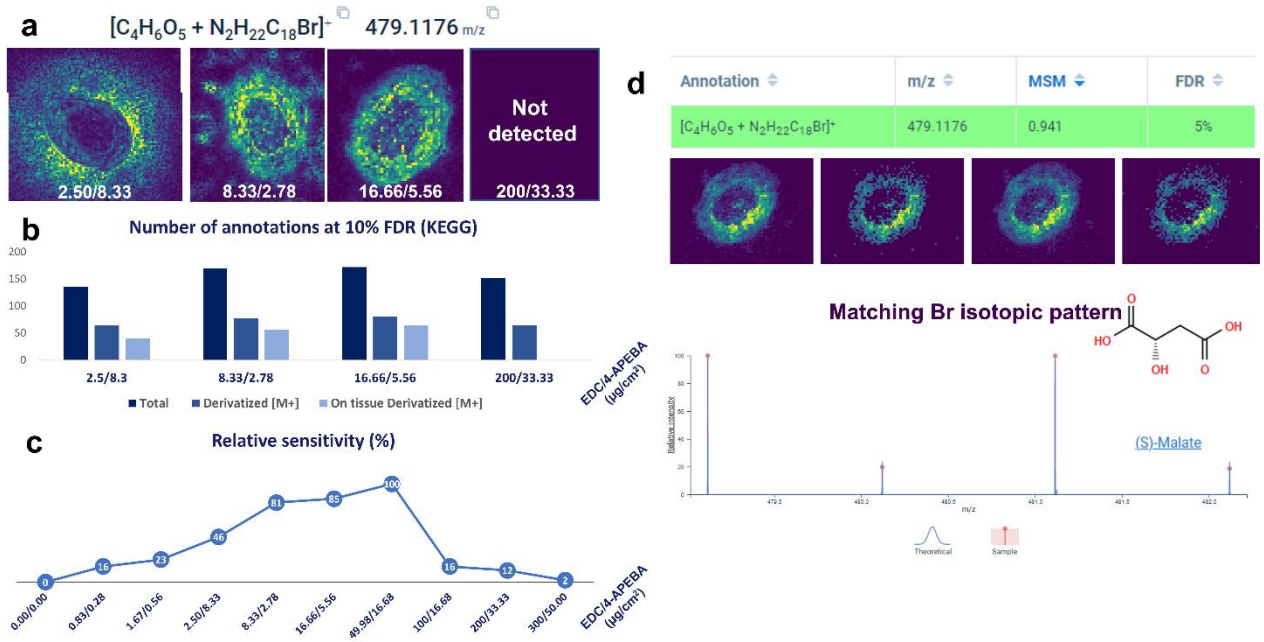

Fig. 3 MALDI-MSI outputs in different EDC/4-APEBA derivatization conditions expressed as EDC (µg/cm²) / 4-APEBA (µg/cm²) demonstrated on poplar root cross section. **a** Delocalization (i.e., leakage of molecules from their native localizations) observed after deposition of EDC and APEBA in water. The derivatized form of malic acid $[C_4H_6O_5+C_{18}H_{22}N_2Br]^+$ is provided as an exemplary molecule used to evaluate delocalization. **b** Number of annotated features retrieved from METASPACE at 10% FDR using KEGG database of these datasets. **c** Sensitivity of analyses expressed as relative intensity of derivatized abscisic acid standard in each condition. **d** Spatial distribution of [malate-4-APEBA]$^+$ isotopologues in the cross section of poplar root. Characteristic isotopic pattern of bromine (^{79}Br and ^{81}Br) can be identified with similar relative abundances (51% and 49%, respectively) aiding in spectral identification of isotopologues, which for low abundant low mass metabolites are otherwise broadly undetected.

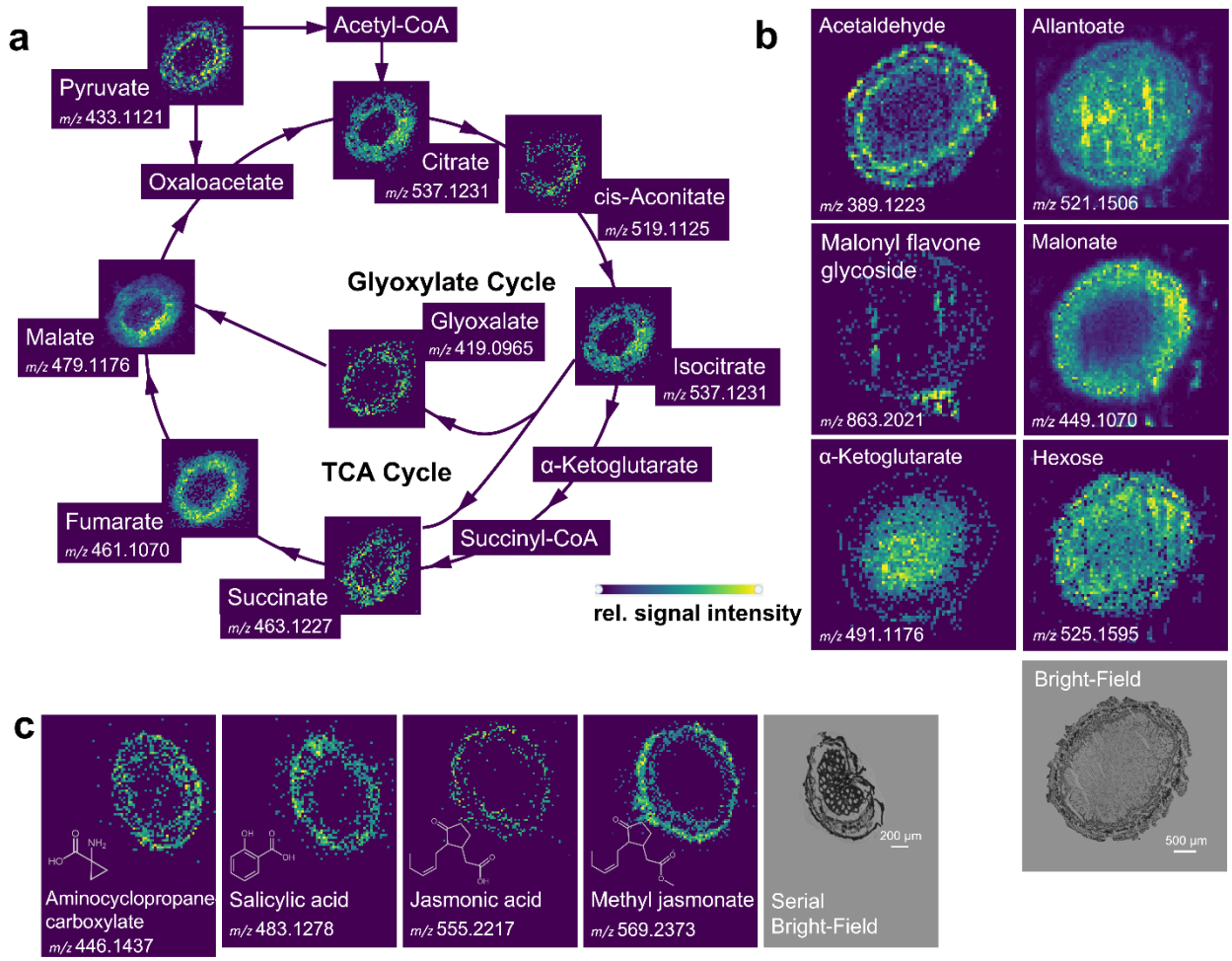

Fig. 4 Spatial distribution of exemplary plant metabolites revealed after on-tissue derivatization with 4-APEBA. All ions were detected as 4-APEBA derivative ion $[M+C_{18}H_{22}N_2Br]^+$. **a** Spatial distribution of multiple components of the TCA and glyoxalate cycle in the cross section of poplar root at 25 µm pixel size. **b** Cell-type specific localization of selected metabolites in the soybean root nodule at 50 µm spatial scale where localizations within the cortex and outer dermal layers can be recognized. A bright-field image of the imaged section is shown. **c** MALDI images of phytohormone distribution in soybean root nodule (upper panel: jasmonic acid and methyl jasmonate) and poplar roots (lower panel: salicylate and aminocyclopropane-carboxylate). A bright-field image of a serial section to that which was imaged is shown.